Published in final edited form as:

Mol Cell. 2017 July 20; 67(2): 228–238.e5. doi:10.1016/j.molcel.2017.05.022.

Sensing Self and Foreign Circular RNAs by Intron Identity

Y. Grace Chen[1], **Myoungjoo V. Kim**[2], **Xingqi Chen**[1], **Pedro J. Batista**[1], **Saeko Aoyama**[2], **Jeremy E. Wilusz**[3], **Akiko Iwasaki**[2], and **Howard Y. Chang**[1,4,*]

[1]Center for Personal Dynamic Regulomes and Program in Epithelial Biology, Stanford University School of Medicine, Stanford, CA 94305, USA

[2]Department of Immunobiology, Howard Hughes Medical Institute, Yale School of Medicine, New Haven, CT 06519, USA

[3]Department of Biochemistry and Biophysics, University of Pennsylvania, Perelman School of Medicine, Philadelphia, PA 19104, USA

SUMMARY

Circular RNAs (circRNAs) are single-stranded RNAs that are joined head to tail with largely unknown functions. Here we show that transfection of purified in vitro generated circRNA into mammalian cells led to potent induction of innate immunity genes and confers protection against viral infection. The nucleic acid sensor RIG-I is necessary to sense foreign circRNA, and RIG-I and foreign circRNA co-aggregate in cytoplasmic foci. CircRNA activation of innate immunity is independent of a 5′ triphosphate, double-stranded RNA structure, or the primary sequence of the foreign circRNA. Instead, self-nonself discrimination depends on the intron that programs the circRNA. Use of a human intron to express a foreign circRNA sequence abrogates immune activation, and mature human circRNA is associated with diverse RNA binding proteins reflecting its endogenous splicing and biogenesis. These results reveal innate immune sensing of circRNA and highlight introns—the predominant output of mammalian transcription—as arbiters of self-nonself identity.

In Brief

*Correspondence: howchang@stanford.edu.
[4]Lead Contact

SUPPLEMENTAL INFORMATION

Supplemental Information includes six figures and three tables and can be found with this article online at http://dx.doi.org/10.1016/j.molcel.2017.05.022.

AUTHOR CONTRIBUTIONS

Conceptualization: Y.G.C. and H.Y.C.; Methodology: Y.G.C. and H.Y.C.; Investigation: Y.G.C. (all except for with HEK293T and MEFs), M.V.K., S.A., and A.I. (293T and MEFs), X.C. (microscopy), and J.E.W. (ChIRP-MS design); Analysis: Y.G.C. (all except for RNA-seq data) and P.J.B. (RNA-seq data); Resources: J.E.W. (*ZKSCAN1* and *laccase2* plasmids); Writing: Y.G.C. and H.Y.C.

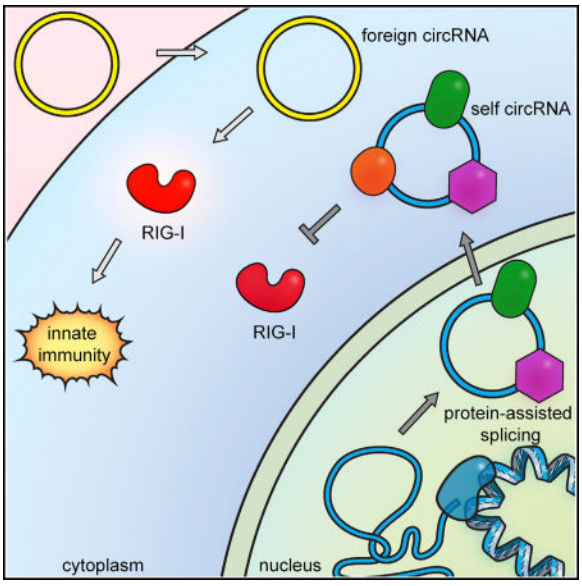

Chen et al. show that exogenous circRNAs trigger an immune response that can protect against viral infection. They find that cells distinguish self from nonself circRNAs based on their biogenesis. CircRNAs spliced by endogenous human spliceosomes associate with many RNA-binding proteins that mark their origin as self molecules.

INTRODUCTION

Initially discovered as pathogen genomes such as hepatitis D virus (HDV) and plant viroids (Kos et al., 1986; Sanger et al., 1976), circRNAs were recently recognized as a pervasive class of noncoding RNAs in eukaryotic cells (Hansen et al., 2013; Memczak et al., 2013; Salzman et al., 2012), generated through back splicing (Chen, 2016; Jeck and Sharpless, 2014; Wilusz, 2016). CircRNAs have been postulated to function as microRNA sponges (Hansen et al., 2013, 2011; Memczak et al., 2013), in cell-to-cell information transfer (Lasda and Parker, 2016), as templates for translation (Legnini et al., 2017; Pamudurti et al., 2017; Yang et al., 2017), or memory due to their extraordinary stability (Fischer and Leung, 2017). However, the ability of exogenous circRNA to activate immune response or inhibit viral infection has not been investigated. We show that circRNA generated from foreign introns potently stimulates immune signaling and inhibits viral infection. Additionally, cells distinguish between self-nonself circRNAs based on the introns from which they were produced, perhaps because mature human circRNAs are associated with diverse RNA binding proteins.

RESULTS

Cell-Free Production of CircRNA by Phage Intron

To generate circRNAs that we could subsequently transfect into cells, we programmed in vitro production of circRNAs with autocatalytic-splicing introns (Figure 1A). The group I intron of phage T4 *thymidylate synthase* (*td*) gene is well characterized to circularize while the exons linearly splice together (Chandry and Belfort, 1987; Ford and Ares, 1994;

Perriman and Ares, 1998). When the *td* intron order is permuted (5′ half placed at the 3′ position and vice versa) flanking any exon sequence, the exon is circularized via two autocatalytic transesterification reactions (Ford and Ares, 1994; Puttaraju and Been, 1995). We encoded destabilized green fluorescent protein (GFP) followed by the encephalomyocarditis virus (EMCV) internal ribosome entry site (IRES) as the exon. Successful circRNA production was monitored by reverse transcription and quantitative polymerase chain reaction (qRT-PCR) analysis with divergent primers (Figure 1A, brown, and Figure S1A) that span the splice junction and only amplifies product when circRNA is present. Convergent primers (Figure 1A, green, and Figure S1A) detect both the linear and circRNA. Circularization also brings the IRES upstream of the GFP sequence, allowing protein translation. Following in vitro transcription, the permuted autocatalytic-splicing introns produce a 1.5 kilobase circRNA, as expected (Figure 1B). As a control, we transcribed a linear RNA with the same sequence as the circRNA and treated both linear and circRNAs with phosphatase so there are no 5′ phosphates present in either sample. The circRNA product is resistant to digestion with the exonuclease RNase R while the linear RNA unspliced transcript and side products were depleted (Figure 1B). We thus used RNase R treatment to purify circRNA in all subsequent experiments. Direct sequencing of the circRNA splice junction confirmed a uniform splice junction, precisely at the expected autocatalytic splice site (Figure 1C). Thus, phage autocatalytic-splicing intron enables in vitro production of circRNAs that may be suitable for mammalian expression.

Exogenous CircRNA Stimulates Innate Immunity Gene Expression

In the course of investigating circRNA as a vehicle for ectopic gene expression, we unexpectedly uncovered its potent immune stimulatory property. When we transiently transfected purified unmodified or Cy3-labeled circRNA into HeLa cells, we observed very little GFP expression and, surprisingly, significantly more cell death in the cells containing circRNA than linear RNA encoding the same sequence (Figure S1B). This effect required intracellular introduction of circRNA via transfection; adding circRNA to the media had no effect. Transfection of in vitro transcribed linear RNA is known to induce innate immune signaling (Warren et al., 2010), but such an effect was not known for circRNAs. RNA-seq of HeLa cells transiently transfected with linear or circRNA showed that circRNA more potently stimulated the expression of genes involved in innate immunity; the top enriched Gene Ontology terms include response to cytokine, regulation of cytokine production, cellular response to virus, and NF-κB signaling (Figure 2A). 127 genes were significantly induced by either linear or circRNA transfection (induced 4-fold, $p < 0.05$, FDR < 0.1), and the majority of these genes were significantly more induced by circRNA than linear RNA transfection (84 observed versus 64 expected by chance alone, $p = 0.00016$, hypergeometric distribution; Figure 2A). CircRNA-induced genes include well-known innate immunity regulators such as retinoic-acid-inducible gene-I (*RIG-I*, also known as *DDX58*), melanoma-differentiation-associated gene 5 (*MDA5*, also known as *IFIH1*), 2′-5′ oligoadenylate synthase 1 (*OAS1*), OAS-like protein (*OASL*), and, to a lesser extent, protein kinase R (*PKR*).

To confirm the RNA-seq results, we transfected linear or circRNA into HeLa cells, washed extensively after 24 hr to remove unincorporated RNA, and isolated total RNA for qRT-

PCR. We measured the expression of a panel of innate immune genes relative to actin and also measured the levels of transfected circular and linear RNAs inside cells for normalization to account for the differences between linear and circRNA transfection efficiency and stability for all subsequent assays (STAR Methods). CircRNA potently stimulates the expression of several innate immunity genes (e.g., ~500-fold for *RIG-I* and 200-fold for *OASL* mRNA) and more potently than linear RNA of the same sequence or mock transfection control (Figures 2B, S1C, S2A, and S2B and Table S1). RIG-I induction by circRNA was also confirmed on the protein level (Figure S2C). Transfection of circRNA also induced innate immunity genes in a keratinocyte cell line (HaCaT; Figure S2D) and a mouse macrophage cell line (RAW 264.7; Figure S2E). These results suggest circRNA is an inducer of innate immunity signaling.

CircRNA Inhibits RNA Virus Infection

To test if the immunogenic response stimulated by circRNA transfection affects the ability of a virus to infect HeLa cells, we first transfected cells with linear or circRNA labeled with Cy3, waited 24 hr, and exposed cells to Venezuelan equine encephalitis virus harboring a green fluorescent protein reporter gene (VEEV-GFP, a +ssRNA virus). FACS analysis showed mock-treated cells and cells with linear RNA were infected to similar levels, while cells transfected with circRNA had a 10-fold lower VEEV-GFP infection rate (Figures 2C and 2D). Additionally in cultures transfected with circRNA, neighbor cells that did not contain transfected circRNA also had decreased infection levels, similar to cells that had circRNA (Figure 2E). This collective, non-cell-autonomous protection from virus infection is consistent with the ability of foreign circRNA to induce antiviral cytokines such as interferon-beta. Collectively, these results show that sensing of exogenous circRNA can confer functional immune protection against a viral pathogen.

RIG-I Mediates Immune Response to Foreign CircRNA

RIG-I and MDA5 are two well-known intracellular sensors of foreign RNAs in mammalian cells. RIG-I is activated by a short “panhandle” RNA structure with 5′ triphosphate (Hornung et al., 2006) while MDA5 is activated by long double-stranded RNAs (Hornung et al., 2006; Kato et al., 2008). Neither of these features is known to exist in circRNA. To investigate which cytosolic foreign nucleic acid sensor may detect exogenous circRNA, we used HEK293T cells that require exogenous RIG-I or MDA5 to be added for sensing exogenous RNAs. We found that expression of RIG-I, but not MDA5, conferred responsiveness to circRNA in HEK293T cells, as evidenced by an ~20-fold induction of *IFNβ-reporter* gene (Figure 3A). Quantitative comparison with low molecular weight polyI:C (range 0.2–1 kb length), which activates RIG-I strongly and MDA5 weakly, showed that accounting for molarity, circRNA is approximately 10-fold more potent than polyI:C in immune gene stimulation. In contrast, MDA5 expression conferred strong responsiveness to long dsRNA but not circRNA, suggesting distinct signaling requirements (Figures S3A–S3C).

Next, we investigated the requirement of RIG-I in sensing circRNA. Transfection of wild-type or *RIG-I* knockout (KO) MEFs (Kato et al., 2005) showed that *RIG-I* KO completely abrogated circRNA-induced innate immune genes (Figure 3B). *RIG-I* KO MEFs are still

inducible by interferon stimulatory DNA, suggesting that *RIG-I* is needed in a proximal step of circRNA sensing (Figure S4A). Similarly, we generated HeLa cells knocked out for human *RIG-I* by CRISPR-Cas9 technology and found that human *RIG-I* KO also substantially reduced the response of innate immunity genes to circRNAs (Figures 3C and S4B). These results suggest that RIG-I is necessary and sufficient to sense foreign circRNA, at least in the cell types examined.

To probe whether RIG-I may directly sense circRNAs, we performed immunofluorescence microscopy of Cy3-labeled transfected RNA and endogenous RIG-I (Figure 3D). We found that RIG-I in cells with transfected circRNA formed more and larger intracellular foci compared to with linear RNA ($p < 0.05$ for each; Figures 3E, S4C, and S4D). Notably, circRNA was significantly more likely to colocalize in RIG-I foci than linear RNA (Figure 3F). The colocalized foci typically have RIG-I signal in the center surrounded by circRNA and are distributed throughout the cytoplasm. These results implicate RIG-I in the proximal sensing of circRNA. Because RIG-I is itself induced by circRNA and needed to sense circRNA, circRNA induction of RIG-I may constitute a positive feedback loop. RIG-I may directly sense circRNA, or it may be required for a proximal signal amplification step for immune gene induction.

Immune Response to CircRNA Is Not Explained by Known Ligands

How might circRNA activate RIG-I? We were able to rule out two possible features. First, the known pathogen-associated molecular pattern (PAMP) for RIG-I includes a 5′ triphosphate on RNA (Hornung et al., 2006). By definition, circRNA does not have a 5′ end, and treatment of our circRNA preparation with phosphatases that selectively cleaves 5′ phosphates did not diminish its ability to stimulate innate immune genes (Figure 4A). As positive control, phosphatase treatment of 5′ triphosphate-containing linear RNA greatly reduced its immune signaling activity (Figure S5A). These results suggest that circRNA activation of RIG-I is not due to contaminating 5′ triphosphates that are present in the circRNA preparation. Second, long double-stranded RNA (dsRNA) can activate immune signaling (typically via MDA5 rather than RIG-I). We tested the possibility that circularization may cause significant differences in secondary structure that lead to innate immune gene activation. We performed in vitro selective 2′-hydroxyl acylation and profiling (SHAPE) experiments, whereby single-stranded bases are mapped by high SHAPE reactivity (Spitale et al., 2015). Sequencing of the SHAPE libraries showed that in vitro-folded linear and circRNA, arising from the same primary sequence, have nearly identical SHAPE reactivity scores, suggesting that they have comparable secondary structures (Figure 4B). There was also no significant difference in the longest consecutive stretch of dsRNA in circular or linear RNA (38 versus 39 bases; Figure 4B). Thus, sensing of circRNA appears independent of known PAMPs of foreign RNAs.

We performed two additional experiments to rule out the possibility that aberrant, unknown products in the preparation of circRNA may cause immune stimulation. First, circRNA generated by in vitro splint ligation (without using the autocatalytic-splicing *td* intron) also induced innate immune genes (Figure 4C), suggesting that any circRNA not generated by mammalian splicing is perceived as foreign. Second, after circRNA production by in vitro

transcription and purification, we used a complementary DNA oligonucleotide and RNase H to specifically cleave the circRNA. Linearization of circRNA abrogated its immune stimulatory property (Figure 4D), indicating that it is indeed the circRNA and not any other product that is responsible for the immune activation. Taken together, these experiments demonstrate that the circular properties of the RNA cause immune gene stimulation.

CircRNA Biogenesis Dictates RNA Activation of Immune Signaling

Next, we mapped the feature of circRNA required to activate innate immune gene expression. We used a phage *td* intron to produce linear and circRNA in vitro containing only the mCherry coding sequence—replacing the entire exonic sequence of GFP-IRES circRNA. The mCherry circRNA potently simulated innate immune genes over linear RNA and control, similar to GFP-IRES circRNA (Figures S5B–S5D). These results suggest that immune activation is based on the circularity of the RNA rather than primary sequence or ribosome binding by IRES. We reasoned that if the circRNA exon does not define "self" versus "foreign," the only remaining feature is the intron that programs the circularization. We transfected a DNA construct that expresses the phage autocatalytic-splicing GFP-IRES circRNA and compared it to a control DNA construct that lacks the second intron half, making it only encode linear RNA. We found that DNA-programmed expression still induced robust immune gene activation, highlighting a potent mode of circRNA induction of immune genes (~600-fold over linear RNA; Figure 5A). We kept the GFP-IRES circRNA exon and replaced the phage *td* intron with endogenous human *ZKSCAN1* introns (Liang and Wilusz, 2014), which do not have autocatalytic-splicing properties (Figures 5A and S6C). Complementary Alu repeats are present in these flanking introns, which enable human *ZKSCAN1* to splice GFP-IRES into a circRNA. The linear control is the vector missing a portion of the upstream *ZKSCAN1* intron so that base pairing of the 5′ and 3′ introns and circularization would not occur. The full-length *ZKSCAN1* introns led to copious production of GFP-IRES circRNA (confirmed by qRT-PCR and used for normalization; Figures S6A and S6B), but completely abrogated innate immune gene induction (Figure 5A). These results suggest that splicing by a "self intron" in human cells confers self-identity to circRNAs irrespective of their exonic sequence, and distinguishes endogenous circRNAs from foreign nucleic acids.

We further interrogated the properties of the foreign circRNA sensing mechanism. First, transfection of a DNA construct encoding the *Drosphila laccase2* introns (Kramer et al., 2015) flanking GFP-IRES exon into HeLa cells programmed circRNA production, as confirmed by qRT-PCR, but did not stimulate innate immune genes (Figure 5B). Thus, because circRNA programmed by *Drosophila* introns but processed by the human spliceosome is sensed as "self," it is likely that the human splicing machinery or an associated process—rather than the sequence of human intron itself—confers self-identity to endogenously produced circRNAs. Second, encoding both *td* and *ZKSCAN1* introns on the same RNA molecule yielded circRNA products that did not activate innate immune genes (Figure 5C). The same result is obtained with human introns either flanking phage intron or nested within phage intron. This result suggests that the "self circRNA" identity conferred by human introns is dominant over the foreign identity. Third, co-expression of *ZKSCAN1* intron-programmed circRNAs and *td* circRNAs in the same cells still led to immune gene

activation, indicating that human intron-mediated protection of immune activation operates solely in *cis* and lacks transitive property (Figure S6D).

Endogenous CircRNA Associated with a Diverse Set of RNA-Binding Proteins

Finally, to understand how endogenous human circRNA may be marked, we performed comprehensive identification of RNA binding proteins by mass spectrometry (ChIRP-MS) (Chu et al., 2015) to compare proteins that are associated with model circular or linear RNAs (Table S2). We transfected HeLa cells with DNA plasmids encoding RNAs with combinations of (i) *ZKSCAN1* or phage *td* introns, which direct protein-assisted splicing or autocatalytic splicing, respectively; (ii) *ZKSCAN1* endogenous exons or the GFP-IRES exon; (iii) control linear RNAs that lack one of the flanking introns required for back splicing or circRNAs with full introns (Figure 6A). The endogenous *ZKSCAN1* circRNA arises from a canonical “forward splice” between exons 2 and 3 and a “back splice” from the 3′ of exon 3 back to the 5′ of exon 2 (Liang and Wilusz, 2014); the mix of forward and back splice typifies most circRNAs (Jeck and Sharpless, 2014; Jeck et al., 2013; Salzman et al., 2012; Wilusz, 2016). After DNA transfection, we performed FISH against *td*-intron programmed *circGFP-IRES* and found the circRNA to be predominantly localized to the cytoplasm. Cells were crosslinked with formaldehyde to trap endogenous complexes; we then used oligonucleotide probes to isolate *ZKSCAN1* or GFP-IRES RNA products, along with their associated proteins. The oligonucleotide probes are directed against the exonic sequences only; hence, this experiment tests the consequence of introns on the subsequent fate of RNA binding proteins that associate with circRNA.

Following mass spectrometry to identify the proteins, we defined enrichment as containing ten or more spectral counts with 4-fold or greater than the RNase-treated negative control. We found that both circular and linear *ZKSCAN1* RNAs are associated with a large and common set of RNA binding proteins (145 of 192 RBPs [75%]) involved in RNA splicing, ribonucleocomplex assembly, and nucleic acid transport (lane 1 versus lane 2 in Figure 6B, and Table S3). The shared RBPs include multiple components of the spliceosome (e.g., U1, U2, and U4/U6/U5 tri-snRNP subunits), the exon junction complex that is deposited as splice junctions (EIF4A3, MGN2, RNPS1), and factors that mediate nuclear export of RNAs (DDX39B, THOC4, XPO5). In addition, we found a set of 36 proteins that are at least 3-fold more enriched on *circZKSCAN1* than linear *ZKSCAN1* RNA (Figure 6C and Table S3). These include MOV10, a RNA helicase required for replication of HDV circRNA genome (Haussecker et al., 2008) and RNA interference (Tomari et al., 2004), components of the nonsense-mediated decay pathway (UPF1, UPF2), RNA *N6*-methyladenosine reader proteins (YTHDF2, YTHDF3) (Dominissini et al., 2012), and the antiviral protein OASL.

To identify proteins associated with RNAs recognized as “self,” we compared *ZKSCAN1* intron-directed linear and circRNAs. Many of the proteins common to the *ZKSCAN1* introns expressing endogenous *ZKSCAN1* exons were also detected in the ChIRP-MS results from *ZKSCAN1* introns expressing a foreign GFP-IRES exon (lane 1 versus lane 3 in Figures 6B and 6C, and Table S3). This demonstrates that the introns direct the placement of RBPs onto the circular and linear RNAs. The proteins unique to *circGFP-IRES* generated by *ZKSCAN1*-directed circularization also overlap with the *circZKSCAN1*, whereas the

circGFP-IRES generated by *td*-directed circularization have very few proteins associated (lane 3 versus lane 5 in Figure 6C, and Table S3). We did not detect RIG-I associated with the autocatalytically spliced circRNA, perhaps suggesting that the interaction is transient and was not captured by the ChIRP-MS.

Thus, a diverse and distinctive set of RBPs associate with endogenously produced human circRNA. Recent identification of m^6A-marked endogenous human circular RNAs is fully consistent with our observation (Molinie et al., 2016; Yang et al., 2017). These results demonstrate that introns program the protein cargos of circular RNAs, and also refine the set of RNA binding proteins that can mark the circRNA as "self."

DISCUSSION

CircRNAs are prevalent in mammalian cells, but much is still unknown about their function, biosynthesis, degradation, and associated cellular machinery. Endogenous messenger RNAs possess features on their ends—the 5′ cap and 3′ polyA tail— that identify them as products of RNA polymerase II. Do circular RNAs escape immune surveillance? Our results suggest a system of self-nonself discrimination for circRNAs, based on the intron that programs the circularization (Figure 6D). This strategy is elegant and general: cells may sense diverse foreign circRNAs, such as HDV and viroids, irrespective of their primary sequence, while not responding to numerous self circRNAs. Another potential advantage of using introns to distinguish self versus foreign circRNAs is that the large size of human introns (spanning multiple kilobases on average) makes it difficult for compact viral genomes to simply incorporate introns in order to mask foreign circRNAs. We speculate that it may be the expansiveness of human "junk DNA" in introns that confers its utility for self-nonself discrimination and thereby defines humanness.

CircRNAs generated by human intron splicing are endowed with numerous RBPs and potentially other features that mark their origin. How exogenous circRNA activates RIG-I, and how one or more factors deposited by human introns prevent RIG-I activation are key questions for future studies. Our discovery of a large family of proteins associated with human-spliced circRNAs opens the door for systematic analyses. The recognition that circRNAs deemed foreign can activate immune signaling raises the question of circRNA involvement in autoimmune diseases. Conversely, exogenous introduction of circRNAs may boost immune activation for therapeutic purposes.

STAR*METHODS

Detailed methods are provided in the online version of this paper and include the following:

- KEY RESOURCES TABLE
- CONTACT FOR REAGENT AND RESOURCE SHARING
- EXPERIMENTAL MODEL AND SUBJECT DETAILS
  - Cell lines
  - Microbe strains

- METHOD DETAILS
  - Plasmids
  - RNA synthesis and purification
  - Reverse transcription and real time PCR analysis (qRT-PCR)
- CELL LINES AND MAINTENANCE
  - Cell Culture and Transient Transfection
  - RNA extraction, selection, library preparation, and sequencing
  - Western blot analysis
  - VEEV-GFP infection
  - Luciferase activity assay
  - Construction and validation of RIG-I$^{-/-}$ in HeLa cells
  - Immunofluorescence
  - ChIRP-mass spectrometry
  - Flow cytometry
- QUANTIFICATION AND STATISTICAL ANALYSIS
  - RNA expression analysis
  - Image analysis
- DATA AND SOFTWARE AVAILABILITY

STAR*METHODS

CONTACT FOR REAGENT AND RESOURCE SHARING

Further information and requests for reagents may be directed to and will be fulfilled by the Lead Contact, Dr. Howard Y. Chang, at Stanford University (howchang@stanford.edu).

EXPERIMENTAL MODEL AND SUBJECT DETAILS

Cell lines—Wild-type and RIG-I KO MEFs were provided by Dr. Shizuo Akira and Dr. Takashi Satoh (Osaka University). MEFs were grown in Dulbecco's modified Eagle's medium (DMEM, 11995-073) supplemented with 100 units/ml penicillin-streptomycin (GIBCO, 15140-163), 10% (v/v) fetal bovine serum and 50 μM 2-Mercaptoethanol (Sigma-Aldrich, 516732). Human HeLa (cervical adenocarcinoma, ATCC CCL-2), human HEK293T (embryonic kidney, ATCC CRL-3216), human HaCaT (immortalized keratinocyte, ATCC PCS-200-010) and mouse RAW 264.7 (macrophage, ATCC TIB-71) cells were grown in Dulbecco's modified Eagle's medium (DMEM, Invitrogen, 11995-073) supplemented with 100 units/ml penicillin-streptomycin (GIBCO, 15140-163) and 10% (v/v) fetal bovine serum (Invitrogen, 12676-011). Cell growth was maintained at 37°C in a 5% CO_2 atmosphere.

Microbe strains—TOP10 *E. coli* competent cells were obtained from ThermoFisher Scientific. Cells were stored at −80°C and grown in LB medium at 37° C.

METHOD DETAILS

Plasmids—The plasmid containing the permuted intron-exon from the *td* gene of T4 bacteriophage was provided by Dr. Manuel Ares, Jr. (University of California, Santa Cruz). Plasmids expressing *ZKSCAN1* and *laccase2* were provided by Dr. Jeremy E Wilusz. *ZKSCAN1* 100–2232 plasmid was used for circRNA production and *ZKSCAN1* 450–2232 plasmid for linear RNA production (Liang and Wilusz, 2014). Gibson assembly (NEB) was used to construct the autocatalytic-splicing and *ZKSCAN1* plasmids containing the GFP-IRES or mCherry exons.

RNA synthesis and purification—Unmodified RNA was synthesized by in vitro transcription using mMessage mMachine T7 transcription kit (Ambion, AM1344) following the manufacturer's instructions. Cy3-labeled RNA was synthesized by in vitro transcription using MEGAscript T7 transcription kit (Ambion, AM1334) and adding Cy3-UTP (GE Healthcare, PA53026) in a 1:25 ratio with the transcription kit's CTP. Transcribed RNA was purified by RNeasy Mini column (QIAGEN), treated with FastAP (ThermoFisher Scientific, EF0652) following the manufacturer's instructions, and purified again by RNeasy Mini column. CircRNA was purified by treatment with RNase R (Epicenter, RNR07250) following the manufacturer's instructions. Splint ligation circRNA was generated by treatment of in vitro transcribed linear RNA and DNA splint ATATGACGCAATATTAAACGGTAGACCCAAGAAAACATCTACTGAG with T4 DNA ligase (Moore, 1999; Moore and Sharp, 1992) (New England Bio, Inc., M0202M), and circRNA was isolated following RNase R treatment. For the RNase H assay, circRNA was hybridized with DNA complementary to the splice junction (ATTAAACGGTAGACCCAAGAAAAC) and treated with RNase H (New England Biolabs Inc., M0297L) following the manufacturer's instructions. Quality of the RNA was assessed by agarose gel or Bioanalyzer (Agilent).

Reverse transcription and real time PCR analysis (qRT-PCR)—Total RNA was isolated from cells using TRIzol (Invitrogen, 15596018) and an RNeasy Mini kit (QIAGEN) following the manufacturer's instructions. qRT-PCR analysis was performed in triplicate using Brilliant II SYBR Green qRT-PCR Master Mix (Agilent, 600825) and a LightCycler 480 (Roche). Primers used found in Table S1. mRNA levels were normalized to actin, GAPDH, or HPRT values. Relative expression of indicated mRNA genes for circRNA transfection are normalized by level of transfected RNA and plotted as the fold change to the expression level of cells with mock or linear RNA transfection. For the luciferase assays, results are presented relative to renilla luciferase activity.

CELL LINES AND MAINTENANCE

Cell Culture and Transient Transfection—1 ug of low molecular weight poly(I:C) (Invivogen, tlrl-picw), high molecular weight poly(I:C) (Invivogen, vac-pic), or interferon stimulatory DNA (Invivogen, tlrl-isdn) were transfected using Lipofectamine 2000 (Invitrogen, 11668-019). Briefly, cells were transfected at 70 to 80% confluence using

Lipofectamine 2000. The nucleic acids and Lipofectamine 2000 were diluted, mixed in Opti-MEM (Invitrogen, 31985-088), and incubated for 5 min at room temperature (RT). Following, the nucleic acids and Lipofectamine 2000 were mixed together, incubated for 15 min at RT and then the nucleic acids-Lipofectamine 2000 complexes were applied to the monolayer cultures. 500 ng of linear or circRNA was transfected into one well of a 24-well plate.

RNA extraction, selection, library preparation, and sequencing—Total RNA was isolated using TRIzol reagent (Invitrogen), according to manufacturer's instructions. RNA was re-suspended in ultrapure water and treated with DNase I (Ambion, AM2222) for 30 min at 37°C and subjected to RNA clean up with RNeasy Midi Kit (QIAGEN), according to manufacturer's instructions. RNA was eluted in ultrapure water. Total RNA was subjected to ribosomal RNA depletion with RiboMinus, and larger RNAs (> 200nt) were enriched by selective binding to RNeasy Mini columns in the following ratio: 100 μL RNA in water to 350 μL RLT to 120 μL of 100% EtOH. The RNeasy manual was followed for washes and elution.

Library preparation for high-throughput sequencing was performed following the library cloning method described in Flynn et al. (Flynn et al., 2015). The following notes are minor deviations for RNA-seq: Ribo-depleted RNA was fragmented to ~100 nt by incubation for 45 s at 95°C with Zinc chloride buffer (10 mM $ZnCl_2$,10mM Tris-HCl, pH 7.0). The reaction was stopped with 0.2M EDTA and immediately placed on ice. The fragmented RNA was recovered using the RNEasy Mini Kit (QIAGEN). Fragmented RNA was treated with 10 Units of T4 PNK (New England Biolabs, Inc., M0201S), 1 Unit of FastAP (ThermoFisher Scientific) in 1x PNK buffer with 40 Units of Ribolock RNase Inhibitor (Life Technologies, EO0384) for 30 min at 37°C, to repair the 3′ of the RNA. For the ligation of the 3′ end adaptor, 0.8 μM of 3′ end biotin blocked preadenylated adaptor, 6.6 Units of T4 RNA ligase 1, high concentration (New England Biolabs, Inc., M0437M), in 1x RNA ligase buffer with 5 mM DTT and 50% PEG8000, were added, and the reaction was incubated at RT for 3 hr. To remove excess linker, 30 Units of RecJf (New England Biolabs, Inc., M0264L) and 20 Units of 5′ Deadenylase (New England Biolabs, Inc., M0331S) in 1x RecJ buffer with Ribolock RNase Inhibitor were added to the reaction, and incubated for 1 hr at 37°C. The reaction was cleaned with RNA Clean & Concentrator columns (Zymo Research, R1016).

Reverse transcription, biotin capture of ligated fragments, cDNA circularization, library amplification, and PAGE purification were carried out exactly as written in the previously published method (Flynn et al., 2015). One microliter of each sample was used for quantification with Kapa Library quantification (Kapa Biosystems) and then sent for sequencing on the Illumina MiSeq for 1 × 50-bp cycle run.

Western blot analysis—HeLa cells were collected and lysed 24 hr after transfection to extract total proteins. RIPA buffer (150 mM sodium chloride, 1% Triton X-100, 0.5% sodium deoxycholate, 0.1% sodium dodecyl sulfate, 50 mM Tris, pH 8.0) was used to lyse the cells. Proteins were fractionated by sodium dodecyl sulfate polyacrylamide gel electrophoresis (SDS-PAGE), transferred to nitrocellulose membranes, blocked in

phosphate-buffer saline containing 3% (wt/vol) nonfat milk for 1 hr at RT, and then incubated overnight at 4°C with the indicated primary antibody. Rabbit polyclonal antibody was used to detect RIG-I (Cell Signaling Technology, 3743S) and goat polyclonal IgG antibody was used to detect actin (Santa Cruz Biotechnology, SC-1616). IRDye 800CW Goat anti-rabbit IgG (LI-COR, 926–32211) or IRDye 680CW Donkey anti-goat IgG (LI-COR, 926–68074) secondary antibodies were used according to the manufacturer's instructions. Western blot detection and quantification was done using an Odyssey infrared imaging system (LI-COR).

VEEV-GFP infection—Transient transfection of linear or circRNA into HeLa cells as described above was performed 24h prior to infection with TC83 vaccine strain VEEV-GFP at MOI of 3.72. Samples were stained with LIVE/DEAD Fixable Blue Dead Cell Stain Kit, for UV excitation (Thermo-Fisher, L23105), 1:500 in PBS +1% FBS for 15 min. Cells were fixed with 4% paraformaldehyde in PBS for 10 min. Cells were processed and analyzed on a special order FACS Aria II (BD Biosciences).

Luciferase activity assay—Luciferase activity was determined by Dual-Luciferase Reporter Assay system (Promega, E1910) following the manufacturer's instructions. Briefly, cultured cells were lysed in the Passive Lysis Buffer. Firefly and renilla luciferase activity in the supernatant was measured with SpectraMax i3x (Molecular Devices) and analyzed with Softmax pro 6.4 (Molecular Devices).

Construction and validation of RIG-I$^{-/-}$ in HeLa cells—CRISPR target sequence of RIG-I was chosen using casoffinder (http://www.rgenome.net/cas-offinder/) to have less than 4 mismatches for NGG PAM sequence. Self-complementary oligonucleotides (acaccgGATTTCTGCTGTTCATACACg and aaaacGTGTATGAACAGCAGAAATCcg, ordered from Elim Biopharm) targeting a portion of DDX58 (GATTTCTGCTGTTCATACAC) were annealed, and ligated into BsmbI-digested MLM3636 (Addgene, 43860) to create a plasmid that would transcribe the guide RNA. 650 ng of MLM3636 containing the DDX58 target sequence and 650 ng of p3s-Cas9HC (Addgene, 43945) were transiently transfected into 24-well plates of HeLa as described above. After 48 hr, colonies were plated in 96-well with a density of 0.3 cells/well for single colony isolation. To validate RIG-I knockout clones, genomic DNA was isolated during sub-culture using DNeasy Blood &Tissue Kit (QIAGEN). DDX58 locus containing the target sequence was amplified by PCR (Forward: GGCTGTTGGCATGCTACTTA, Reverse: CCTTAGCACAGAGCCTGACA, and nested Forward: TCAGCTCAGTGGTATTAGAAGAGC, nested Reverse: TGTGCCACGTAAACATCAAA) followed by T7 Endonuclease I (New England Biolabs Inc., M0302L) digestion. Clones with appropriate T7 Endonuclease I activity were sequenced by MiSeq (Illumina), after amplifying by PCR (Forward: GGGGAAAGTTGTCTTTTTTGC, Reverse: TACCTACCCATGTCTTTCAAAGTATT) followed by True-seq adaptor ligation. Clones that did not contain an in-frame deletion or wild-type sequence in the MiSeq sequencing were probed by western blot to assess for the presence of RIG-I protein.

Immunofluorescence—HeLa cells were grown on 8-well Nunc® Lab-Tek® Chamber Slide system (Sigma-Aldrich, C7182-1CS) and transient transfection of Cy3-RNA was performed as described above. At 80%–90% confluency, cells were fixed with 1% formaldehyde (Sigma-Aldrich) for 10 min at RT. The formaldehyde fixed slide was rinsed in PBS and permeabilized in PBS 0.5% Triton X-100 for 10 min at RT. Then, the slide was blocked with antibody dilution reagent (ThermoFisher Scientific, 00–3218) for 1 hr at RT. Rabbit polyclonal primary antibody anti-RIG-I (Cell Signaling Technology, 3743S) was diluted in antibody dilution reagent 1:500, and incubated overnight at 4°C. After washing with PBS containing 0.05% Tween-20 for 3 times, 10 min each, slides were incubated with secondary antibodies goat antirabbit -Atto647N (Sigma-Aldrich, 50185-1ML-F), for 45 min at RT. The slides were washed with PBS containing 0.05% Tween-20 for 3 times 10 min each, mounted using Vectashield with DAPI (Vector Labs, H-1200) and imaged with Leica SP8.

ChIRP-mass spectrometry—ChIRP-mass spectrometry was conducted as previously described in Chu et al.(Chu et al., 2015). Probes used are found in Table S2. Spectral counts ten and above with four or more times enrichment over the RNase control were used. All samples were filtered for proteins found in the CRAPome(Mellacheruvu et al., 2013) and normalized to the signal of CRAPome proteins to account for difference in instrument running conditions. Mass spectrometry was conducted at the Vincent Coates Foundation Mass Spectrometry Laboratory, Stanford University Mass Spectrometry. GO term enrichment was calculated with Metascape (Tripathi et al., 2015; http://metascape.org).

Flow cytometry—Cells were stained with Annexin V-FITC (BD PharMingen, 556420) following the manufacturer's instructions. Cells were processed and analyzed on a special order FACS Aria II (BD Biosciences).

QUANTIFICATION AND STATISTICAL ANALYSIS

RNA expression analysis—Libraries were separated by barcode, matching reads were collapsed and barcodes removed. For all libraries, single-end RNA-Seq reads were initially mapped against human ribosomal RNA. Reads aligning to the rRNA were discarded, and remaining reads were mapped to the human (hg19 assembly) genome using STAR (Dobin et al., 2013). Reads for each transcript were extracted using HTSeq (Anders et al., 2015). Differential gene expression was calculated with DESeq2 (Love et al., 2014). GO term enrichment was calculated with Metascape (Tripathi et al., 2015; http://metascape.org).

Image analysis—Images were taken under Leica SP8 and the colocalization analysis was performed in Volocity software (PerkinElmer). In brief, the signal intensity and area from both Cy3 and RIG-I were measured in the Volocity Measurement function, and the intersection of the two channels was used to defined overlapping area. Overlapping fraction was calculated with following equation: Overlapping fraction = interest area / total area from two channels. RIG-I foci density was calculated with the following equation: number of RIG-I foci detected / number of cells. ~45 cells with independent replicates were measured and p value was calculated using Student's t test.

DATA AND SOFTWARE AVAILABILITY

The accession number for the sequencing data reported in this paper is Gene Expression Omnibus database: GSE81345.

Supplementary Material

Refer to Web version on PubMed Central for supplementary material.

Acknowledgments

We thank Dr. Shizuo Akira and Dr. Takashi Satoh at Osaka University for providing wild-type and RIG-I$^{-/-}$ MEFs, and Dr. Jan Carette and Dr. Jennifer Lumb at Stanford University for providing VEEV-GFP virus. We thank Byron Lee for technical help and members of our labs for discussion. We thank Vincent Coates Foundation Mass Spectrometry Laboratory, Stanford University Mass Spectrometry for mass spectrometry. This work was supported by Dean's Fellowship and National Institutes of Health Postgraduate Training Program 2T32AR00742231 (Y.G.C.), James Hudson Brown-Alexander Brown Coxe Fellowship (M.V.K.), Swedish Research Council International Postdoctoral Fellowship VR-2016-06794 (X.C.), Damon Runyon Cancer Research Foundation 2090-11 and National Institutes of Health Postgraduate Training Program 2T32AR00742231 (P.J.B.), Rita Allen Foundation Scholar (J.E.W.), Howard Hughes Medical Institute (A.I.), National Institutes of Health (R00-GM104166 and R35-GM119735 to J.E.W.; R41AI120269 to A.I.; P50-HG007735 and R01-HG004361 to H.Y.C.), and Parker Institute for Cancer Immunotherapy (H.Y.C.). Stanford University has filed a patent based on this work, and Y.G.C. and H.Y.C. are named inventors.

References

Anders S, Pyl PT, Huber W. HTSeq-a Python framework to work with high-throughput sequencing data. Bioinformatics. 2015; 31:166–169. [PubMed: 25260700]

Chandry PS, Belfort M. Activation of a cryptic 5′ splice site in the upstream exon of the phage T4 td transcript: exon context, missplicing, and mRNA deletion in a fidelity mutant. Genes Dev. 1987; 1:1028–1037. [PubMed: 3322941]

Chen L-L. The biogenesis and emerging roles of circular RNAs. Nat. Rev. Mol. Cell Biol. 2016; 17:205–211. advance online publication. [PubMed: 26908011]

Chu C, Zhang QC, da Rocha ST, Flynn RA, Bharadwaj M, Calabrese JM, Magnuson T, Heard E, Chang HY. Systematic discovery of Xist RNA binding proteins. Cell. 2015; 161:404–416. [PubMed: 25843628]

Dobin A, Davis CA, Schlesinger F, Drenkow J, Zaleski C, Jha S, Batut P, Chaisson M, Gingeras TR. STAR:ultrafast universal RNA-seq aligner. Bioinformatics. 2013; 29:15–21. [PubMed: 23104886]

Dominissini D, Moshitch-Moshkovitz S, Schwartz S, Salmon-Divon M, Ungar L, Osenberg S, Cesarkas K, Jacob-Hirsch J, Amariglio N, Kupiec M, et al. Topology of the human and mouse m6A RNA methylomes revealed by m6A–seq. Nature. 2012; 485:201–206. [PubMed: 22575960]

Fischer JW, Leung AKL. CircRNAs: a regulator of cellular stress. Crit. Rev. Biochem. Mol. Biol. 2017; 52:220–233. [PubMed: 28095716]

Flynn RA, Martin L, Spitale RC, Do BT, Sagan SM, Zarnegar B, Qu K, Khavari PA, Quake SR, Sarnow P, Chang HY. Dissecting noncoding and pathogen RNA-protein interactomes. RNA. 2015; 21:135–143. [PubMed: 25411354]

Ford E, Ares M Jr. Synthesis of circular RNA in bacteria and yeast using RNA cyclase ribozymes derived from a group I intron of phage T4. Proc. Natl. Acad. Sci. USA. 1994; 91:3117–3121. [PubMed: 7512723]

Hansen TB, Wiklund ED, Bramsen JB, Villadsen SB, Statham AL, Clark SJ, Kjems J. miRNA-dependent gene silencing involving Ago2-mediated cleavage of a circular antisense RNA. EMBO J. 2011; 30:4414–4422. [PubMed: 21964070]

Hansen TB, Jensen TI, Clausen BH, Bramsen JB, Finsen B, Damgaard CK, Kjems J. Natural RNA circles function as efficient microRNA sponges. Nature. 2013; 495:384–388. [PubMed: 23446346]

Haussecker D, Cao D, Huang Y, Parameswaran P, Fire AZ, Kay MA. Capped small RNAs and MOV10 in human hepatitis delta virus replication. Nat. Struct. Mol. Biol. 2008; 15:714–721. [PubMed: 18552826]

Hornung V, Ellegast J, Kim S, Brzózka K, Jung A, Kato H, Poeck H, Akira S, Conzelmann K-K, Schlee M, et al. 5′-Triphosphate RNA is the ligand for RIG-I. Science. 2006; 314:994–997. [PubMed: 17038590]

Jeck WR, Sharpless NE. Detecting and characterizing circular RNAs. Nat. Biotechnol. 2014; 32:453–461. [PubMed: 24811520]

Jeck WR, Sorrentino JA, Wang K, Slevin MK, Burd CE, Liu J, Marzluff WF, Sharpless NE. Circular RNAs are abundant, conserved, and associated with ALU repeats. RNA. 2013; 19:141–157. [PubMed: 23249747]

Kato H, Sato S, Yoneyama M, Yamamoto M, Uematsu S, Matsui K, Tsujimura T, Takeda K, Fujita T, Takeuchi O, Akira S. Cell type-specific involvement of RIG-I in antiviral response. Immunity. 2005; 23:19–28. [PubMed: 16039576]

Kato H, Takeuchi O, Mikamo-Satoh E, Hirai R, Kawai T, Matsushita K, Hiiragi A, Dermody TS, Fujita T, Akira S. Length-dependent recognition of double-stranded ribonucleic acids by retinoic acid-inducible gene-I and melanoma differentiation-associated gene 5. J. Exp. Med. 2008; 205:1601–1610. [PubMed: 18591409]

Kos A, Dijkema R, Arnberg AC, van der Meide PH, Schellekens H. The hepatitis delta (delta) virus possesses a circular RNA. Nature. 1986; 323:558–560. [PubMed: 2429192]

Kramer MC, Liang D, Tatomer DC, Gold B, March ZM, Cherry S, Wilusz JE. Combinatorial control of Drosophila circular RNA expression by intronic repeats, hnRNPs, and SR proteins. Genes Dev. 2015; 29:2168–2182. [PubMed: 26450910]

Lasda E, Parker R. Circular RNAs Co-Precipitate with Extracellular Vesicles: A Possible Mechanism for circRNA Clearance. PLoS ONE. 2016; 11:e0148407. [PubMed: 26848835]

Legnini I, Di Timoteo G, Rossi F, Morlando M, Briganti F, Sthandier O, Fatica A, Santini T, Andronache A, Wade M, et al. Circ-ZNF609 Is a Circular RNA that Can Be Translated and Functions in Myogenesis. Mol. Cell. 2017; 66:22–37.e9. [PubMed: 28344082]

Liang D, Wilusz JE. Short intronic repeat sequences facilitate circular RNA production. Genes Dev. 2014; 28:2233–2247. [PubMed: 25281217]

Love MI, Huber W, Anders S. Moderated estimation of fold change and dispersion for RNA-seq data with DESeq2. Genome Biol. 2014; 15:550. [PubMed: 25516281]

Mellacheruvu D, Wright Z, Couzens AL, Lambert J-P, St-Denis NA, Li T, Miteva YV, Hauri S, Sardiu ME, Low TY, et al. The CRAPome: a contaminant repository for affinity purification-mass spectrometry data. Nat. Methods. 2013; 10:730–736. [PubMed: 23921808]

Memczak S, Jens M, Elefsinioti A, Torti F, Krueger J, Rybak A, Maier L, Mackowiak SD, Gregersen LH, Munschauer M, et al. Circular RNAs are a large class of animal RNAs with regulatory potency. Nature. 2013; 495:333–338. [PubMed: 23446348]

Molinie B, Wang J, Lim KS, Hillebrand R, Lu ZX, Van Wittenberghe N, Howard BD, Daneshvar K, Mullen AC, Dedon P, et al. m(6)ALAIC-seq reveals the census and complexity of the m(6)A epitranscriptome. Nat. Methods. 2016; 13:692–698. [PubMed: 27376769]

Moore MJ. Joining RNA molecules with T4 DNA ligase. Methods Mol. Biol. 1999; 118:11–19. [PubMed: 10549511]

Moore MJ, Sharp PA. Site-specific modification of pre-mRNA: the 2′-hydroxyl groups at the splice sites. Science. 1992; 256:992–997. [PubMed: 1589782]

Pamudurti NR, Bartok O, Jens M, Ashwal-Fluss R, Stottmeister C, Ruhe L, Hanan M, Wyler E, Perez-Hernandez D, Ramberger E, et al. Translation of CircRNAs. Mol. Cell. 2017; 66:9–21.e7. [PubMed: 28344080]

Perriman R, Ares M Jr. Circular mRNA can direct translation of extremely long repeating-sequence proteins in vivo. RNA. 1998; 4:1047–1054. [PubMed: 9740124]

Puttaraju M, Been MD. Generation of nuclease resistant circular RNA decoys for HIV-Tat and HIV-Rev by autocatalytic splicing. Nucleic Acids Symp. Ser. 1995; 33:49–51.

Salzman J, Gawad C, Wang PL, Lacayo N, Brown PO. Circular RNAs are the predominant transcript isoform from hundreds of human genes in diverse cell types. PLoS ONE. 2012; 7:e30733. [PubMed: 22319583]

Sanger HL, Klotz G, Riesner D, Gross HJ, Kleinschmidt AK. Viroids are single-stranded covalently closed circular RNA molecules existing as highly base-paired rod-like structures. Proc. Natl. Acad. Sci. USA. 1976; 73:3852–3856. [PubMed: 1069269]

Spitale RC, Flynn RA, Zhang QC, Crisalli P, Lee B, Jung J-W, Kuchelmeister HY, Batista PJ, Torre EA, Kool ET, Chang HY. Structural imprints in vivo decode RNA regulatory mechanisms. Nature. 2015; 519:486–490. [PubMed: 25799993]

Tomari Y, Du T, Haley B, Schwarz DS, Bennett R, Cook HA, Koppetsch BS, Theurkauf WE, Zamore PD. RISC assembly defects in the Drosophila RNAi mutant armitage. Cell. 2004; 116:831–841. [PubMed: 15035985]

Tripathi S, Pohl MO, Zhou Y, Rodriguez-Frandsen A, Wang G, Stein DA, Moulton HM, DeJesus P, Che J, Mulder LC, et al. Meta-and Orthogonal Integration of Influenza "OMICs" Data Defines a Role for UBR4 in Virus Budding. Cell Host Microbe. 2015; 18:723–735. [PubMed: 26651948]

Warren L, Manos PD, Ahfeldt T, Loh YH, Li H, Lau F, Ebina W, Mandal PK, Smith ZD, Meissner A, et al. Highly efficient reprogramming to pluripotency and directed differentiation of human cells with synthetic modified mRNA. Cell Stem Cell. 2010; 7:618–630. [PubMed: 20888316]

Wilusz, JE. [Published online August 29, 2016] Circular RNAs: Unexpected outputs of many protein-coding genes. RNA Biol. 2016. http://dx.doi.org/10.1080/15476286.2016.1227905

Yang Y, Fan X, Mao M, Song X, Wu P, Zhang Y, Jin Y, Yang Y, Chen LL, Wang Y, et al. Extensive translation of circular RNAs driven by N(6)-methyladenosine. Cell Res. 2017; 27:626–641. [PubMed: 28281539]

Highlights

- Exogenous circRNA potently stimulates immune signaling, and circRNA co-aggregate with RIG-I
- Transfected cells with exogenous circRNA have increased protection against viral infection
- Self-nonself discrimination depends on the intron that programs the circRNA
- Mature human circRNA associated with diverse RNA-binding proteins

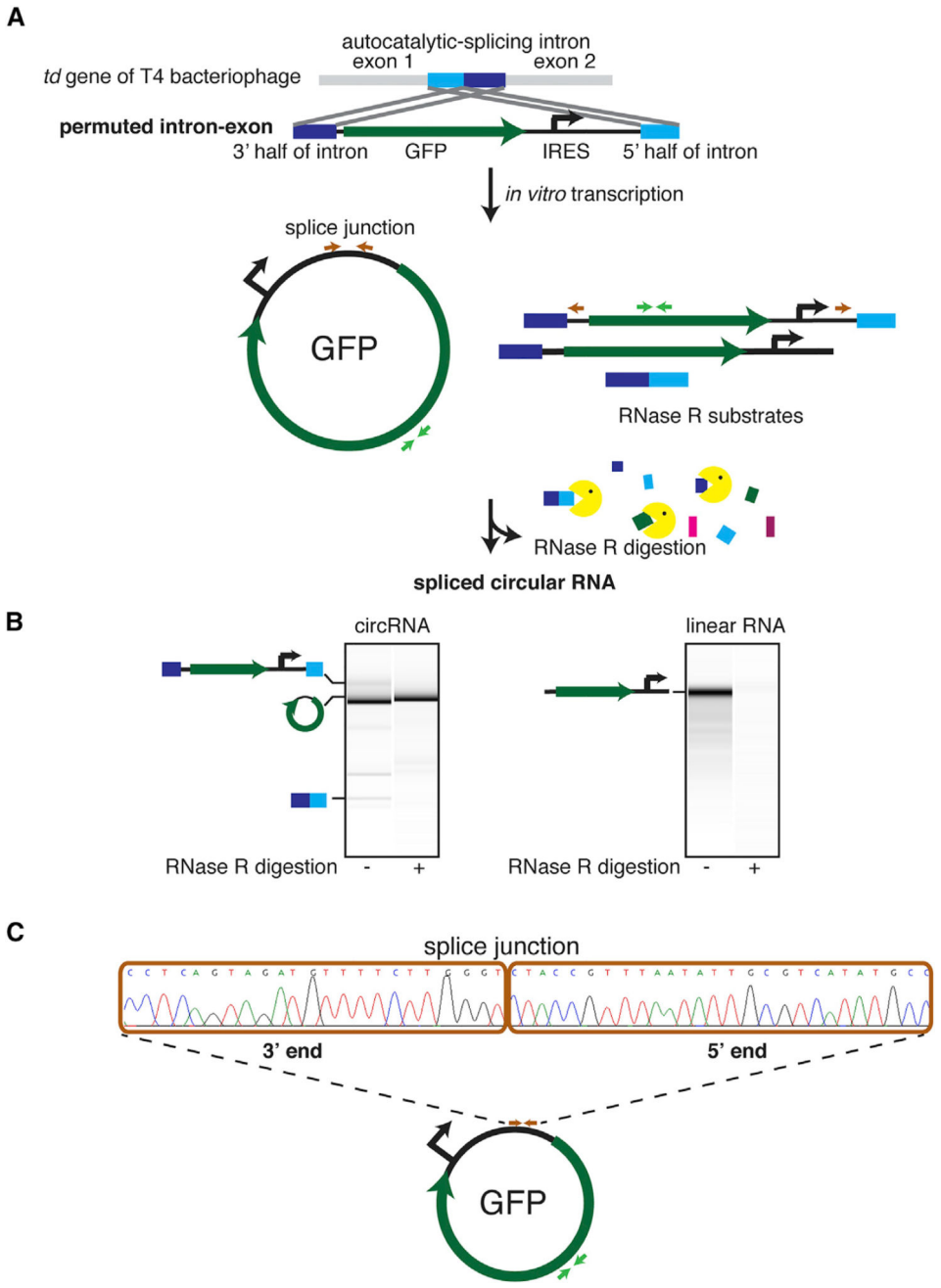

Figure 1. Cell-Free Production of CircRNA

(A) CircRNA was synthesized by in vitro transcription from a permuted intron-exon template. RNase R treatment of the transcription products enriched for circRNA. Green arrows represent the convergent qRT-PCR primers to detect both linear and circRNA; brown arrows represent the divergent qRT-PCR primers to detect circRNA.

(B) Linear and circRNA were treated with RNase R and analyzed by Bioanalyzer.

(C) Sequencing of circRNA product reveals precise and uniform splice junction.

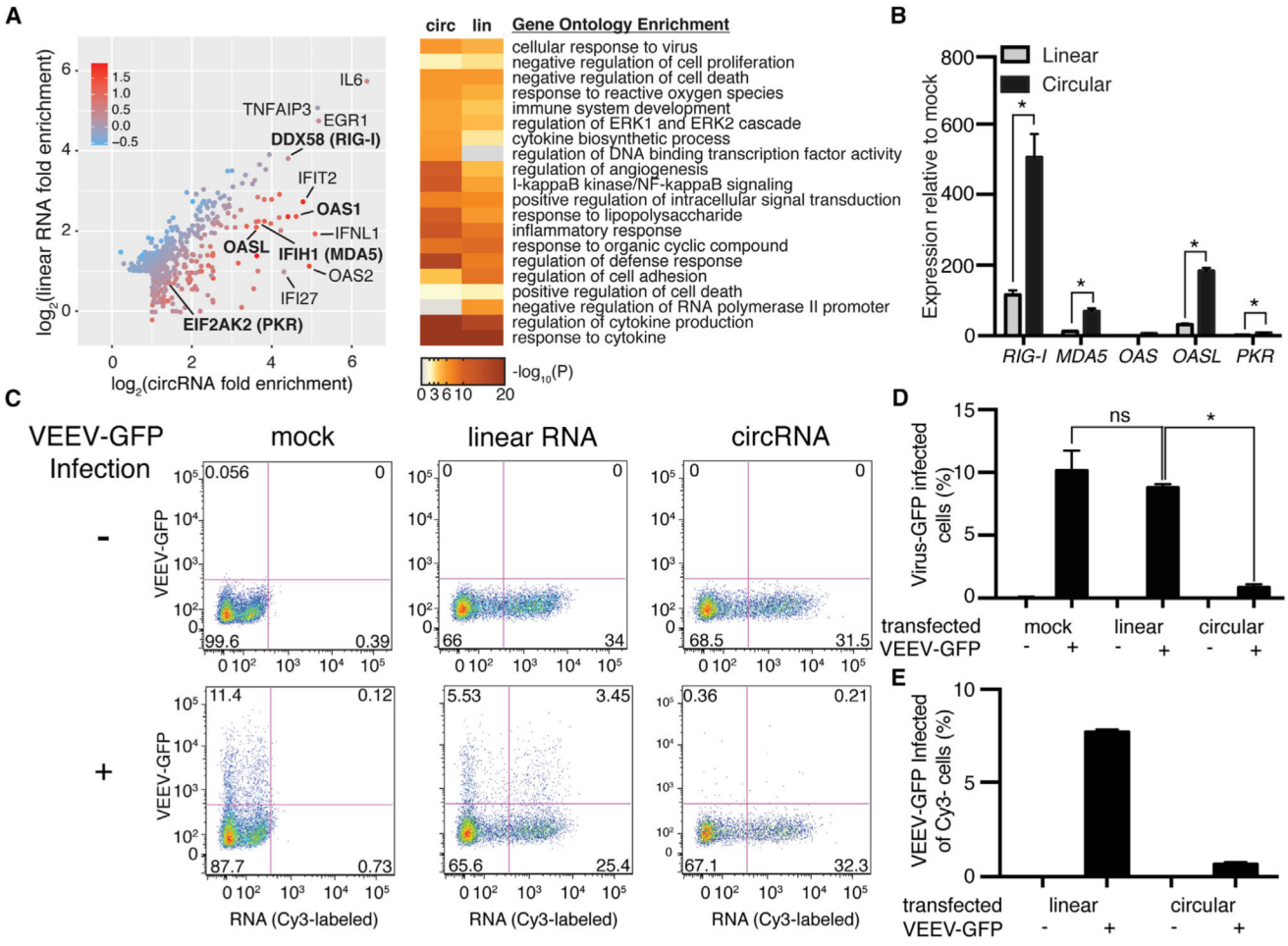

Figure 2. Exogenous CircRNA Stimulates Innate Immunity Gene Expression and Inhibits Viral Infection

(A) Linear and circRNA stimulate expression of specific genes. Left: scatterplot of RNA-seq result of HeLa cells transfected with linear or circRNA encoding GFP-IRES sequence. Genes induced by at least 2-fold compared to mock control are plotted, and the color scale represents the enrichment of circRNA compared to linear RNA. Genes shown in bold were validated by qRT-PCR below. Right: Gene Ontology enrichment of genes induced by circular or linear RNA. Heatmap GO enrichment p value is shown.

(B) CircRNA stimulates expression of innate immune genes. HeLa cells were mock transfected or transfected with 500 ng of linear or circRNA encoding GFP-IRES. Relative expression of the indicated mRNA and transfected RNA are measured by qRT-PCR. Means ± SEM are shown (n = 3), *$p < 0.05$, Student's t test, throughout.

(C) CircRNA transfection protects against viral infection. FACS analysis plots of HeLa cells transfected with 500 ng of Cy3-labeled linear or circRNA and exposed to VEEV-GFP virus.

(D) Percent of all HeLa cells infected with VEEV-GFP following transfection with linear or circRNA.

(E) Percent of HeLa cells that did not contain Cy3-labeled linear or circRNA infected with VEEV-GFP following transfection with linear or circRNA.

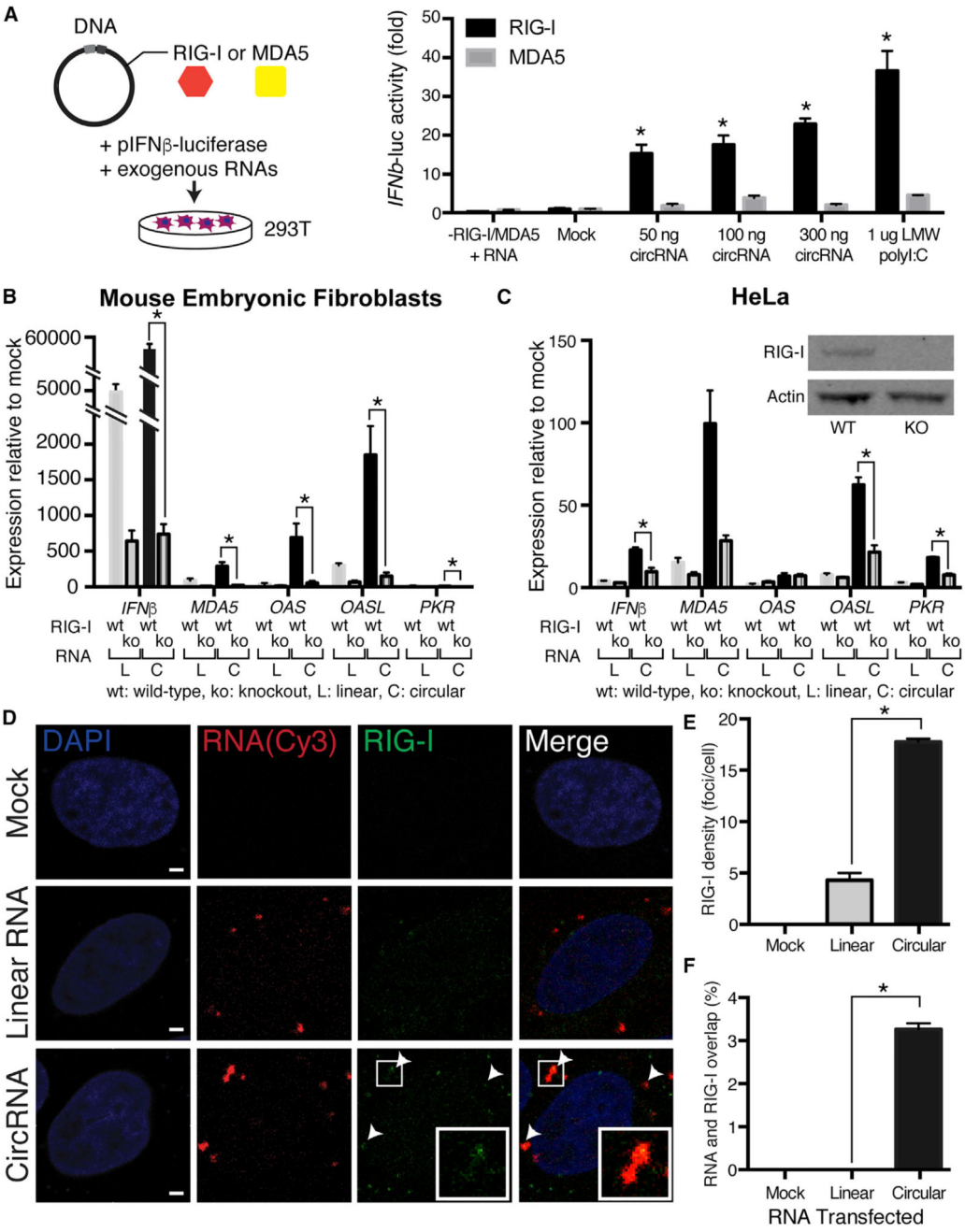

Figure 3. RIG-I Is Necessary and Sufficient to Sense Exogenous CircRNA

(A) RIG-I but not MDA-5 confers circRNA sensitivity in HEK293T cells. Luciferase activity of HEK293T cells transfected with plasmids encoding RIG-I or MDA5, along with mouse *Ifnb* promoter-firefly luciferase/*Renilla* luciferase vectors, and the indicated circRNA ligands or LMW polyI:C as positive control. Cells transfected with RIG-I or MDA5 only (mock) were used as a negative control. Results are presented relative to *Renilla* luciferase activity (*$p < 0.05$ compared to mock control and for RIG-I over MDA5).

(B) RIG-I is required to sense transfected circRNA in MEFs. Wild-type or RIG-I knockout (KO) MEFs were mock transfected or transfected with 500 ng of linear or circRNA. Relative

expression of the indicated mRNA and transfected RNA are measured by qRT-PCR. Means ± SEM are shown (n = 3); *p < 0.05 throughout.

(C) RIG-I is required to sense transfected circRNA in HeLa cells. Wild-type or RIG-I knockout (KO) HeLa were mock transfected or transfected with 500 ng of linear or circRNA. Relative expression of the indicated mRNA and transfected RNA are measured by qRT-PCR. Means ± SEM are shown (n = 3). Inset: western blot of RIG-I or actin from wild-type or KO HeLa cells.

(D) CircRNA transfection induces RIG-I foci. HeLa cells were transfected with 500 ng of Cy3-labeled linear or circRNA encoding GFP-IRES and costained for RIG-I. Subcellular distribution of Cy3-labeled RNA (red), RIG-I (detected with secondary antibody conjugated with -Atto647N, pseudo-colored green), and 4′,6′-diamidino-2-phenylindole (DAPI)-stained nuclei (blue) were visualized by confocal microscopy. Scale bar, 2 μm. White arrows indicate areas of RIG-I and RNA colocalization.

(E) Quantification of the RIG-I density. Means ± SEM are shown; n ≈ 41 cells for each condition.

(F) Quantification of the overlap fraction between RIG-I and linear or circRNA. Means ± SEM are shown; n ≈ 41 cells for each condition.

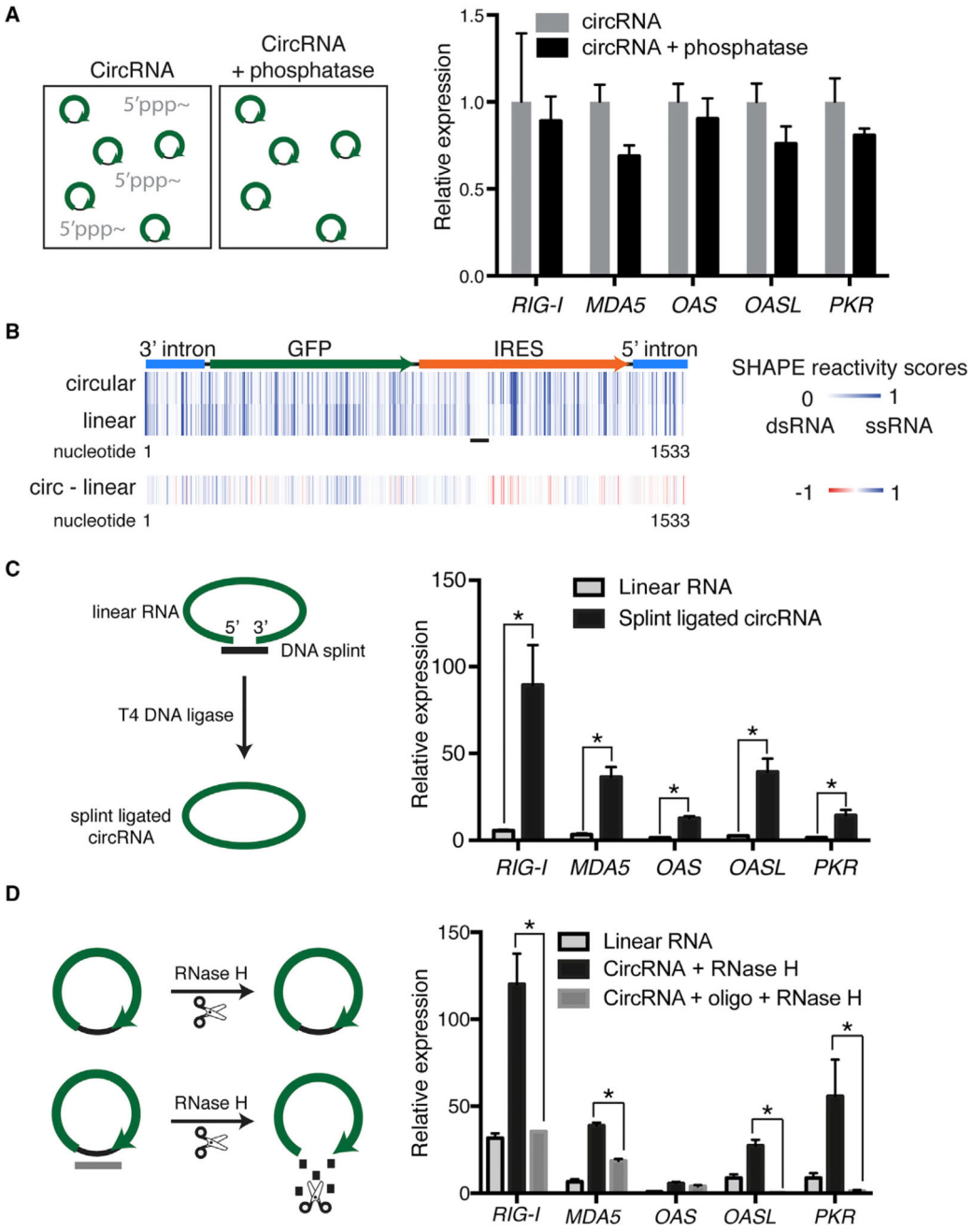

Figure 4. CircRNA Stimulation of Innate Immune Genes Is Not Explained by Known RIG-I Ligands

(A) Exogenous circRNA does not contain 5′ triphosphate. HeLa cells were transfected with 500 ng of circRNA or circRNA treated with phosphatase. Relative expression of the indicated mRNA and transfected RNA are measured by qRT-PCR. Means ± SEM are shown (n = 3).

(B) Exogenous circRNA does not contain long dsRNA duplex. In vitro selective 2′-hydroxyl acylation analyzed by primer extension (SHAPE) was conducted on linear and circRNA. SHAPE reactivity scores were calculated for each nucleotide. Black line denotes the longest consecutive dsRNA region.

(C) Transfection of circRNA made from ligating the ends of linear RNA stimulates innate immune genes. HeLa cells were mock transfected or transfected with 500 ng of linear or splint ligated circRNA encoding GFP-IRES. Relative expression of the indicated mRNA and transfected RNA are measured by qRT-PCR. Means ± SEM are shown (n = 3); *p < 0.05 throughout.

(D) CircRNA samples do not contain aberrant products that stimulate immune response. CircRNA was treated with RNase H in the presence of hybridizing oligonucleotide. HeLa cells were mock transfected or transfected with linear RNA, circRNA, or circRNA treated with RNase H and hybridizing oligonucleotide. Relative expression of the indicated mRNA and transfected RNA are measured by qRT-PCR. Means ± SEM are shown (n = 3).

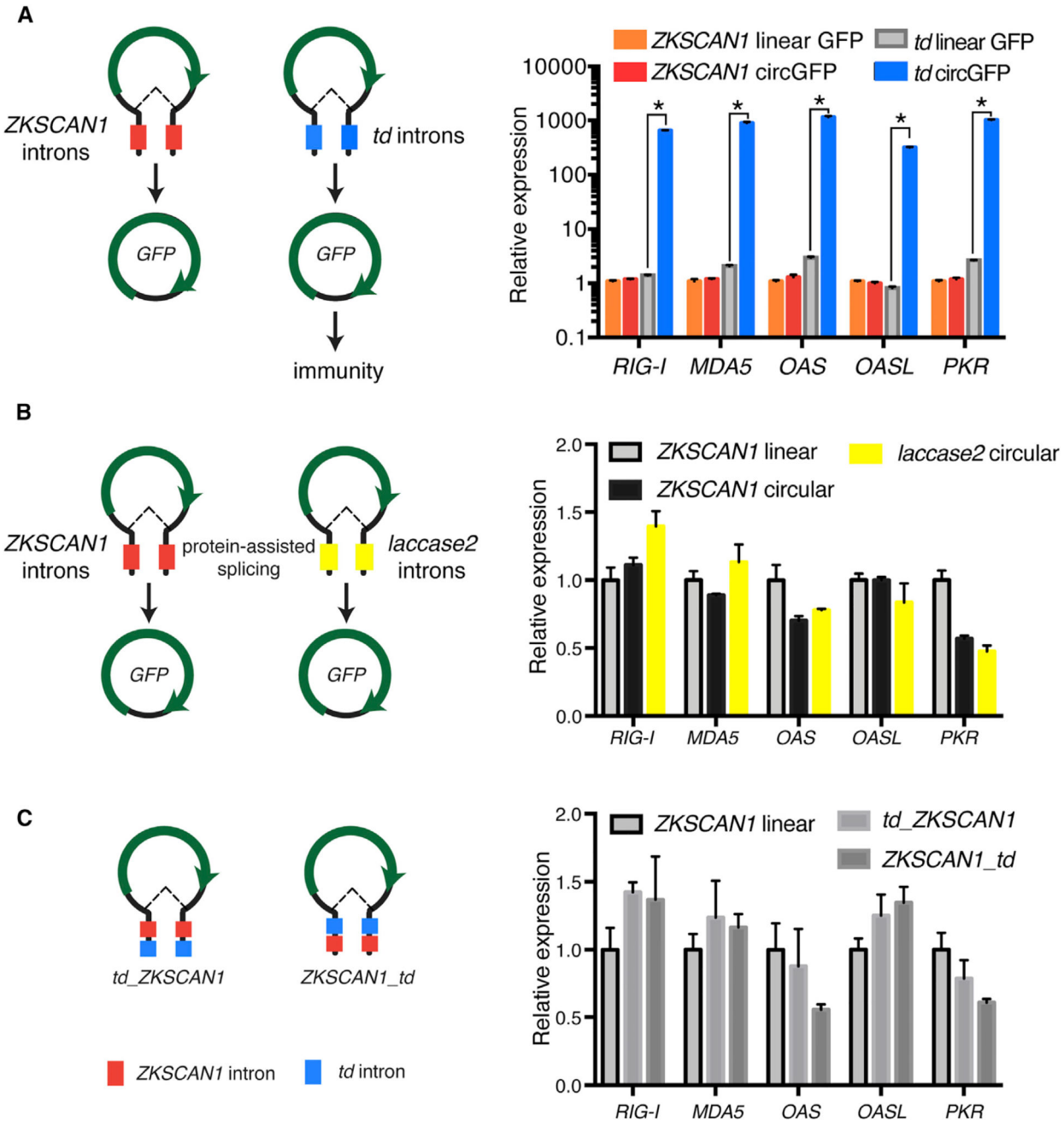

Figure 5. Intron Sequence Determines Immune Signaling by CircRNA

(A) HeLa cells were transfected with 500 ng of DNA plasmid programming *ZKSCAN1* or *td* introns that produce a linear RNA or circRNA encoding GFP-IRES. Relative expression of the indicated mRNA and transfected RNA are measured by qRT-PCR. Means ± SEM are shown (n = 3); *p < 0.05 throughout.

(B) CircRNA produced from *Drosophila laccase2* introns flanking GFP-IRES exon does not stimulate innate immune genes. HeLa cells were transfected with 500 ng of DNA plasmid that produce a linear RNA or circRNA encoding GFP-IRES directed by *laccase2* introns.

(C) Co-expression of programmed protein-assisted and autocatalytic-splicing *td* circRNA still stimulates innate immune genes. HeLa cells were transfected with 500 ng of DNA plasmid programming *ZKSCAN1* intron or sequential *ZKSCAN1* and *td* introns encoding circRNA GFP-IRES. Relative expression of the indicated mRNA and transfected RNA are measured by qRT-PCR, to confirm both the autocatalytic-splicing and protein-assisted splicing processes occur. Means ± SEM are shown (n = 3).

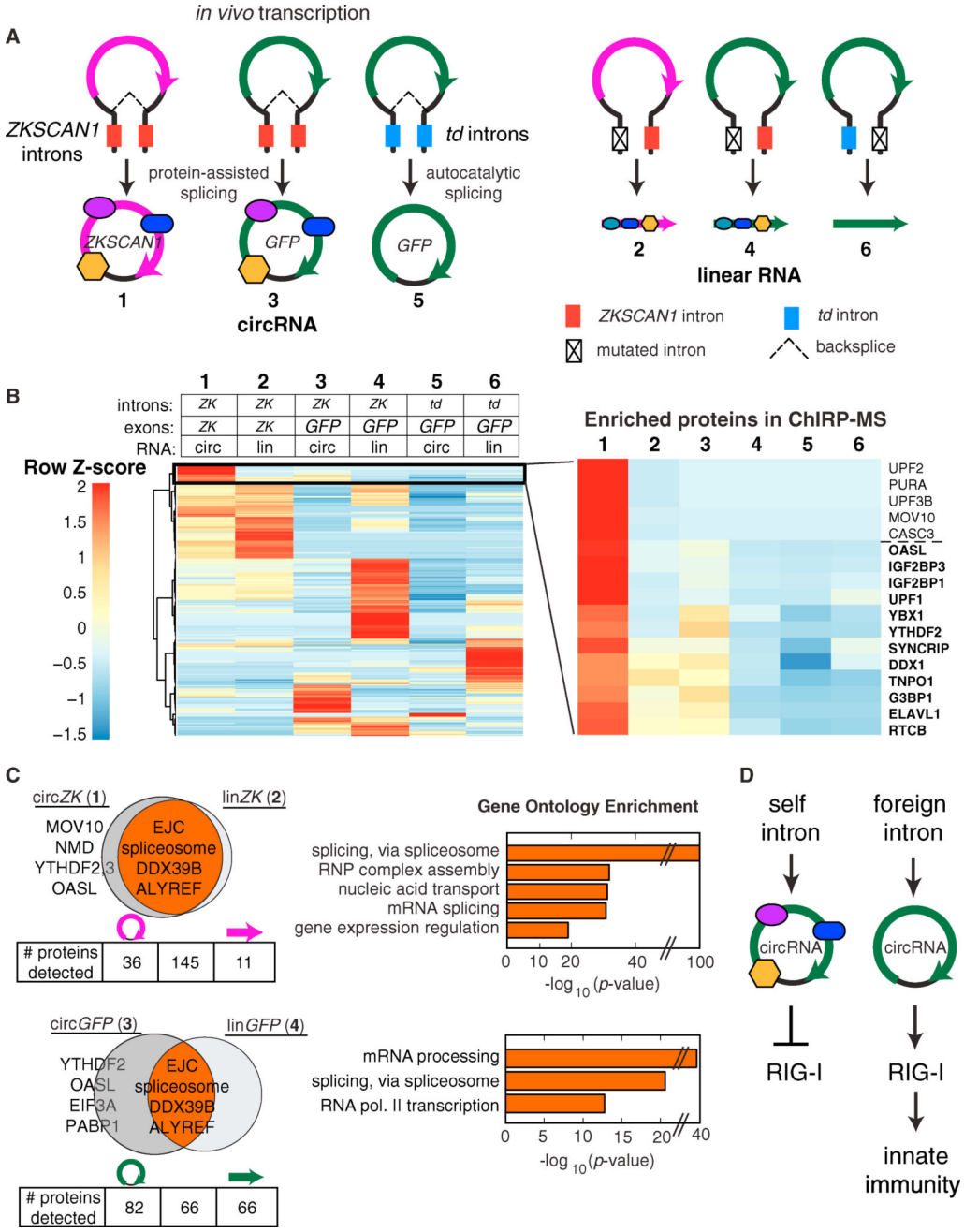

Figure 6. Splicing Mechanism Determines Self versus Non-self CircRNA

(A) Schematic for DNA-programmed splicing of linear or circular *ZKSCAN1* or *td*-directed RNA with endogenous *ZKSCAN1* or GFP-IRES exons.

(B) Heatmap of associated proteins identified by ChIRP-MS for each of the spliced RNAs. Enlarged portion of the heatmap shows the proteins for the most enriched circ*ZKSCAN1* RNAs generated by *ZKSCAN1* introns. Proteins shown in bold are found enriched in *ZKSCAN1* intron-directed circRNAs (both *ZKSCAN1* and GFP-IRES exons).

(C) Proteomic analysis of linear and circRNA ribonucleoprotein complexes. Venn diagrams show enriched proteins detected by ChIRP-MS of *ZKSCAN1* intron-directed linear or

circular *ZKSCAN1* or GFP-IRES exons. Gene ontology enrichment for the proteins detected in both linear and circular *ZKSCAN1* or GFP-IRES samples.
(D) Model of self versus non-self discrimination of mammalian circRNAs.

KEY RESOURCES TABLE

REAGENT or RESOURCE	SOURCE	IDENTIFIER
Antibodies		
Rabbit polyclonal anti-RIG-I	Cell Signaling Technology	3743S; RRID: AB_2269233
Goat polyclonal IgG anti-actin	Santa Cruz Biotechnology	SC-1616; RRID: AB_630836
IRDye 800CW Goat anti-rabbit IgG	LI-COR	926–32211; RRID: AB_621843
IRDye 680CW Donkey anti-goat IgG	LI-COR	926–68074; RRID: AB_10956736
Secondary antibody goat anti-rabbit -Atto647N	Sigma-Aldrich	50185-1ML-F
Bacterial and Virus Strains		
TC83 vaccine strain VEEV-GFP	Dr. Jan Carette	N/A
Chemicals, Peptides, and Recombinant Proteins		
Cy3-UTP	GE Healthcare	PA53026
FastAP	ThermoFisher Scientific	EF0652
RNase R	Epicenter	RNR07250
T4 DNA ligase	New England Biolabs	M0202M
RNase H	New England Biolabs	M0297L
DNase I	Ambion	AM2222
T4 PNK	New England Biolabs	M0201S
Ribolock RNase Inhibitor	Life Technologies	EO0384
T4 RNA ligase 1, high concentration	New England Biolabs	M0437M
RecJf	New England Biolabs	M0264L
Deadenylase	New England Biolabs	M0331S
T7 Endonuclease I	New England Biolabs	M0302L
TRIzol	Invitrogen	15596018
Brilliant II SYBR Green qRT-PCR Master Mix	Agilent	600825
Low molecular weight poly(I:C)	Invivogen	tlrl-picw
High molecular weight poly(I:C)	Invivogen	vac-pic
Interferon stimulatory DNA	Invivogen	tlrl-isdn
Lipofectamine 2000	Invitrogen	11668-019
Antibody dilution reagent	ThermoFisher Scientific	00-3218
DAPI	Vector Labs	H-1200
Annexin V-FITC	BD PharMingen	556420
Critical Commercial Assays		
mMessage mMachine T7 transcription kit	Ambion	AM1344
MEGAscript T7 transcription kit	Ambion	AM1334
RiboMinus Eukaryote Kit for RNA-Seq	Invitrogen	A1083708
LIVE/DEAD Fixable Blue Dead Cell Stain Kit	ThermoFisher	L23105
Dual-Luciferase Reporter Assay	Promega	E1910
Deposited Data		

REAGENT or RESOURCE	SOURCE	IDENTIFIER
Raw and analyzed RNA-seq data	This paper	GEO: GSE81345
ChIRP-MS data	This paper	Table S1
Experimental Models: Cell Lines		
HeLa	ATCC	CCL-2
HEK293T	ATCC	CRL-3216
HaCaT	ATCC	PCS-200-010
RAW 264.7	ATCC	TIB-71
Wild-type MEF	Kato et al., 2005	N/A
RIG-I KO MEF	Kato et al., 2005	N/A
RIG-I KO HeLa	This paper	N/A
Oligonucleotides		
Primers	This paper	Table S2
ChIRP probes	This paper	Table S3
Recombinant DNA		
Plasmid: autocatalytic-splicing linear GFP-IRES	This paper	N/A
Plasmid: autocatalytic-splicing circular GFP-IRES	This paper	N/A
Plasmid: autocatalytic-splicing linear mCherry	This paper	N/A
Plasmid: autocatalytic-splicing circular mCherry	This paper	N/A
Plasmid: ZKSCAN1-directed linear GFP-IRES	This paper	N/A
Plasmid: ZKSCAN1-directed circular GFP-IRES	This paper	N/A
Plasmid: laccase2-directed linear GFP-IRES	This paper	N/A
Plasmid: laccase2-directed circular GFP-IRES	This paper	N/A
Plasmid: ZKSCAN1-directed linear exon2_intron_exon3	Liang and Wilusz, 2014	N/A
Plasmid: ZKSCAN1-directed circular exon2_intron_exon3	Liang and Wilusz, 2014	N/A
Plasmid: MLM3636	Addgene	43860
Plasmid: p3s-Cas9HC	Addgene	43945
Software and Algorithms		
DESeq2	Love et al., 2014	N/A
Metascape	Tripathi et al., 2015; http://metascape.org	N/A